


Dynamics of a compound droplet under the combined influence of electric field and shear flow

Manash Pratim Borthakur 

Department of Engineering Mechanics, KTH Royal Institute of Technology, Stockholm SE 10044, Sweden

Binita Nath

Institute for Complex Systems, National Research Council, Rome 00185, Italy

Gautam Biswas *

Department of Mechanical Engineering, Indian Institute of Technology Kanpur, Kanpur 208016, India



(Received 13 July 2020; accepted 28 January 2021; published 9 February 2021)

We present a numerical investigation on the dynamics of a compound droplet under the combined influence of an applied electric field and shear flow. The paper is carried out by solving the electro-hydrodynamic equations in a two-dimensional framework, and the interface is captured using a volume-of-fluid approach. Both perfect dielectric as well as leaky dielectric fluids are considered. For the case of dielectric fluids, the deformation of both the inner and outer interfaces can be modulated by either variation of the permittivity contrast between the fluids or the applied field strength. The nature of the polarization forces acting at both the interfaces can be either compressive or tensile depending on the magnitude of the permittivity ratio. The investigations for leaky dielectric fluids reveal that the ratio of electrical permittivity and conductivity between the two phases plays a critical role in deciding the magnitude of deformation and orientation of the compound droplet. The variation of charge accumulated at the interfaces modifies the behavior of the Coulombic forces thereby fundamentally altering the droplet deformation and orientation characteristics. Furthermore, it is demonstrated that the electric field can be suitably applied to engender breakup of the compound droplets.

DOI: [10.1103/PhysRevFluids.6.023603](https://doi.org/10.1103/PhysRevFluids.6.023603)

I. INTRODUCTION

A compound droplet is essentially composed of a drop of one liquid (inner core) encapsulated by another immiscible drop (outer shell). With the advancement of microfluidic technologies, compound droplets have shown promising potential for applications such as next-generation targeted drug delivery [1], material processing [2], and phase separation [3], to name a few. The unique morphology of the compound droplet makes it an ideal candidate for processes involving encapsulation and material screening, and as a template for the synthesis of colloids with structured interiors [4,5]. It is evident that while in some of the applications the breakup of the compound droplet is preferred, in other applications, the stability of the droplet is favored. The success of such technologies strongly relies on the accurate and reliable control of the spatiotemporal hydrodynamic behavior of compound droplets.

The introduction of an electro-hydrodynamic (EHD) force by the application of an electric field provides an efficient pathway to control the motion, deformation, and breakup of droplets [6–8].

*gtm@iitk.ac.in

The presence of the external electric field modifies the stresses acting at the interface, thereby radically altering the behavior of the droplets. A host of commercially important technologies relies on electro-hydrodynamic manipulation for efficient and tunable control of droplets [9,10].

The hydrodynamics of compound droplets in quiescent flows have been studied both theoretically [11,12] and experimentally [13] by previous researchers. A comprehensive review on the fluid mechanics of compound droplets in quiescent flow has been provided by Johnson and Sadhal [14]. Additionally, a wide variety of flow configurations has been explored, including the behavior of compound droplets in extensional and linear flows [15–17], effect of surfactants [18], heat transfer with phase change [19], spreading on partially wetting substrates [20], and motion through capillaries [21]. In particular, the dynamics of compound droplets in shear flow have been investigated by several experimental [22,23] and numerical studies [24–26]. Furthermore, the effect of uniform electric field on the dynamics of compound droplets under quiescent conditions has been analyzed in recent years [27–31].

However, the relevant investigations suggest that the influence of an external electric field on the dynamics of compound droplets in shear flow is heretofore absent in literature. Due to the combined effect of the imposed shear and the applied electric field, a profound influence on the drop dynamics is expected. In view of this, in the present paper, we emphasize understanding the complex interplay of electro-hydrodynamic forces acting on compound droplets in shear flow subjected to an external electric field. By employing a computational fluid dynamics framework, the roles of the applied electric field strength as well as the fluid properties on the droplet morphology and breakup characteristics are investigated in detail, which serves as an addition to the existing literature on compound droplets.

The rest of the paper is organized as follows. The formulation of the problem and the methodology adopted for the simulations are outlined in Sec. II. The validation of the present numerical methodology is also discussed. The obtained results are presented and analyzed in Sec. III. Finally, the conclusions from the paper are briefly summarized in Sec. IV.

II. FORMULATION OF THE PROBLEM

We consider a two-component compound droplet placed inside a channel of length L and height $2H$. The properties of the inner drop fluid and the continuous ambient fluid are considered to be the same, thereby simplifying the hydrodynamics to a two-phase interfacial flow problem. Initially, the outer and inner interfaces are considered as concentric spheres of radius r_i and r_o , respectively. The fluids are considered to be incompressible, Newtonian, and mutually immiscible. Figure 1(a) shows the schematic representation of the computational domain. A Cartesian coordinate system (x, y) is employed with the origin coinciding with the initial drop center. The top and bottom walls move opposite to each other at a constant velocity thereby creating a shear flow. The walls of the channel act as electrodes by maintaining a constant potential difference to generate a uniform electric field.

Under the influence of imposed shear and the electric field, the drops deviate from their initial spherical configuration. Figure 1(b) illustrates the parameters taken into consideration to quantify the morphology of the deformed compound drop. The maximum and minimum distances of the deformed drop interfaces from the origin are termed as L_{\max} and L_{\min} , respectively. The angle which the major axis of the drop makes with the x axis is denoted by θ . The minimum distance between the drop interfaces is denoted by d_{\min} . The deformations of both the inner and outer drops are quantified by introducing the deformation index $D = (L_{\max} - L_{\min}) / (L_{\max} + L_{\min})$.

A. Governing equations

The governing equations pertaining to this problem are discussed below. The hydrodynamics are governed by the incompressible Navier-Stokes and continuity equations. An EHD model is

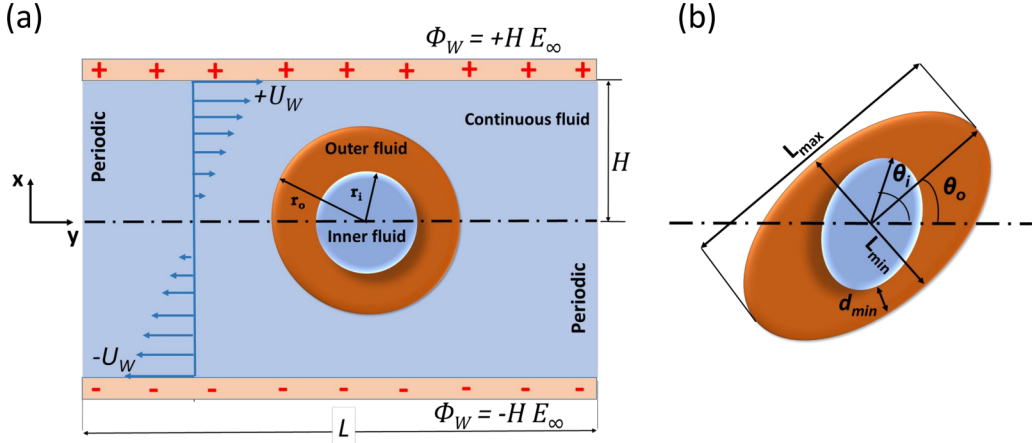


FIG. 1. (a) Schematic of a compound drop inside a channel. The top and bottom walls move opposite to each other at a constant velocity, thereby creating a shear flow. The walls of the channels act as electrodes and a uniform electric field is applied by maintaining a constant potential difference between the electrodes. (b) The maximum and minimum distances of the deformed drop interface from its center are termed as L_{\max} and L_{\min} , respectively. The angle which the major axis of the drop makes with the x axis is denoted by θ . Here, θ_i and θ_o denote the orientation of inner and outer drop, respectively. The minimum distance between the two drop interfaces is quantified by d_{\min} .

adopted to describe the influence of the electric field. The motion of the interface is captured using a volume-of-fluid framework by solving an additional advection equation [32]:

$$\nabla \cdot \mathbf{V} = 0, \quad (1)$$

$$\rho[\partial \mathbf{V} / \partial t + (\mathbf{V} \cdot \nabla) \mathbf{V}] = -\nabla P + \nabla \cdot [\mu(\nabla \mathbf{V} + \nabla \mathbf{V}^T)] + \Gamma \kappa \mathbf{n} \delta + \nabla \cdot \mathbf{M}, \quad (2)$$

$$\partial \alpha / \partial t + \nabla \cdot (\mathbf{V} \alpha) = 0, \quad (3)$$

where $\mathbf{V} = (u, v)$ denotes the velocity field and pressure is represented by p . The fluid viscosity is designated as μ . The surface tension Γ is assumed to be spatially uniform and constant with time. The influence of surface tension is incorporated into the momentum equations employing the continuum surface force model of Brackbill *et al.* [33], where κ is the curvature of the interface, given as $\kappa = -\nabla \cdot \mathbf{n}$, wherein \mathbf{n} is the unit normal to the interface. Maxwell's stress tensor for the electric field \mathbf{M} is defined as $\mathbf{M} = \epsilon[\mathbf{E} \otimes \mathbf{E} - \frac{1}{2}(\mathbf{E} \cdot \mathbf{E})\mathbf{I}]$, wherein ϵ represents the absolute permittivity of the fluid. The volume fraction is denoted by α with values of 1 and 0 inside the outer fluid and inner fluid (as well as continuous fluid), respectively.

The Gauss law of electrostatics can be written in terms of the electric displacement vector \mathbf{D} as $\nabla \cdot \mathbf{D} = \nabla \cdot (\epsilon \mathbf{E}) = q$. Here, q represents the volume density of free charges inside the domain. The irrotational ($\nabla \times \mathbf{E} = 0$) electric field \mathbf{E} can be written in terms of the electric potential (ϕ) as $\mathbf{E} = -\nabla \phi$. Hence, Gauss law can be rewritten in terms of electric potential as $\nabla \cdot (\epsilon \nabla \phi) = -q$. In perfect dielectrics, no free charge carriers exist ($q = 0$) and the Gauss law simplifies to $\nabla \cdot (\epsilon \mathbf{E}) = \nabla \cdot (\epsilon \nabla \phi) = 0$.

For the case of leaky dielectric fluids, a small but finite amount of charge carriers exists in the domain. The charge conservation equation for volumetric charge density is given by

$$\partial q / \partial t + \nabla \cdot (q \mathbf{V}) = -\nabla \cdot (\sigma \mathbf{E}). \quad (4)$$

Here, σ represents the electrical conductivity of the fluid. However, the assumption of leaky dielectric fluid presumes that the time scale of charge relaxation is much smaller than the flow

time scale. As a consequence, the free charges present in the bulk migrate and accumulate at the fluid-fluid interface instantaneously. The bulk fluid effectively remains free of charges and the charge transport almost exclusively occurs at the interface [18].

The electrostatic force acting on leaky dielectric fluids is given by

$$\mathbf{f}_e = \nabla \cdot \mathbf{M} = -\frac{1}{2} \mathbf{E} \cdot \mathbf{E} \nabla \epsilon + q \mathbf{E}. \quad (5)$$

However, for perfect dielectric fluids, the electrostatic force (\mathbf{f}_e) acting on the fluids can be written as

$$\mathbf{f}_e = \nabla \cdot \mathbf{M} = -\frac{1}{2} \mathbf{E} \cdot \mathbf{E} \nabla \epsilon. \quad (6)$$

The fluid properties are volume averaged as

$$\rho = \rho_o \alpha + \rho_c (1 - \alpha), \quad (7)$$

$$\mu = \mu_o \alpha + \mu_c (1 - \alpha), \quad (8)$$

$$\epsilon = \epsilon_o \alpha + \epsilon_c (1 - \alpha), \quad (9)$$

$$\sigma = \sigma_o \alpha + \sigma_c (1 - \alpha), \quad (10)$$

where subscripts c and o denote the continuous fluid (as well as inner fluid) and outer fluid, respectively.

B. Initial and boundary conditions

The simulations are initialized by placing a concentric compound droplet in a quiescent fluid. No-slip and no penetration conditions are imposed at the rigid channel walls and the flow is assumed to be periodic along the horizontal direction. The shear driven flow is generated by continuously moving the upper and lower walls with velocity $+U_W$ and $-U_W$, respectively. Here, $\mathbf{U}_w = (\pm GH, 0)$, where G is the shear rate.

The external electric field is applied by imposing constant voltage boundary conditions, i.e., $\pm\phi_w$ at the upper and lower walls of the channel, respectively. Here, $\phi_w = HE_\infty$, wherein E_∞ denotes the magnitude of the applied electric field.

C. Numerical method

We employ an open source parallelized code BASILISK for performing the numerical simulations [34]. The code features an incompressible Navier-Stokes solver with second order accuracy in space and time. The governing equations are discretized using the finite volume technique. The interface between the two phases is captured with a volume-of-fluid framework. A well-balanced and consistent formulation is employed to model the effect of surface tension, which minimizes spurious currents at the interface [34,35]. Furthermore, we include the EHD toolbox provided in the code architecture to simulate the influence of the applied electric field. The chosen solver is considered to be an ideal choice for our paper and has been deployed for simulating a wide variety of fluid flow problems [6,34,36].

D. Scaling

The results from our simulations have been presented in terms of dimensionless parameters. Lengths are scaled by the radius of the outer drop r_o , velocities are scaled by Gr_o , and the material properties of continuous fluid (or inner fluid) are taken as reference values. The electric field strength and charge density are scaled by E_∞ and $\epsilon_c E_\infty / r_o$, respectively. From the above nondimensional-

ization scheme, the dimensionless groups describing the flow are presented in Eq. (11):

$$\begin{aligned} \text{Ca} &= \frac{\mu_c G r_o}{\Gamma}, & \text{Re} &= \frac{\rho_c G r_o^2}{\mu_c}, & \eta &= \frac{\rho_o}{\rho_c}, & \lambda &= \frac{\mu_o}{\mu_c}, & A &= \frac{r_i}{r_o}, \\ S &= \frac{\epsilon_o}{\epsilon_c}, & R &= \frac{\sigma_o}{\sigma_c}, & \text{Ca}_e &= \frac{\epsilon_c E_\infty^2 r_o}{\Gamma}, & \text{Re}_e &= \frac{\epsilon_c G}{\sigma_c}. \end{aligned} \quad (11)$$

The capillary number (Ca) denotes the relative magnitude of viscous over capillary stresses. The Reynolds number (Re) stands for the ratio of inertia over viscous forces. The shell thickness ratio (A) compares the relative size of the inner drop to the outer drop. The electric capillary number (Ca_e) symbolizes the relative strength of electric force over surface tension force. The electric Reynolds number (Re_e) denotes the ratio of charge relaxation to convection time scales. In addition, the dimensionless property ratios are density ratio (η), viscosity ratio (λ), permittivity ratio (S), and conductivity ratio (R). Thus, the dimensionless forms of the governing equations are given as

$$\nabla \cdot \mathbf{V} = 0, \quad (12)$$

$$\text{Re} \rho [\partial \mathbf{V} / \partial t + (\mathbf{V} \cdot \nabla) \mathbf{V}] = -\nabla P + \nabla \cdot [\mu (\nabla \mathbf{V} + \nabla \mathbf{V}^T)] + \frac{1}{\text{Ca}} \kappa \mathbf{n} \delta + \frac{\text{Ca}_e}{\text{Ca}} \nabla \cdot \mathbf{M}, \quad (13)$$

$$\partial \alpha / \partial t + \nabla \cdot (\mathbf{V} \alpha) = 0, \quad (14)$$

$$\nabla \cdot (\epsilon \nabla \phi) = -q, \quad (15)$$

$$\partial q / \partial t + \nabla \cdot (q \mathbf{V}) = -\frac{1}{\text{Re}_e} \nabla \cdot (\sigma \mathbf{E}). \quad (16)$$

E. Validation and grid convergence study

In order to test the accuracy of our numerical formulation, we compare our results with previous investigations. The first order analytical solution for a spherical droplet in a uniform electric field was developed by Taylor [37] as

$$D = \frac{9\text{Ca}_e}{16S(2+R')^2} \left[S(R'^2 + 1) + 3(R'S - 1) \frac{2\lambda + 3}{5\lambda + 5} - 2 \right], \quad (17)$$

where $R' = \frac{1}{R}$ is the ratio of electrical resistivity of the fluids. Figure 2(a) shows the deformation of a static droplet suspended in a system under uniform electric field with $S = 2.0$, $R = 2.5$, and $\lambda = 1.0$. The analytical predictions of Taylor [37] are in good quantitative agreement with our numerical results. However, a slight deviation is observed at higher Ca_e due to the fact that the analytical solutions are derived under the assumption of small deformation conditions. Figure 2(b) presents the steady shape of a compound droplet subjected to shear flow, in the absence of an electric field. The operating parameters are $\eta = \lambda = 1$, $\text{Re} = 0.1$, $\text{Ca} = 0.3$, and $A = 0.5$. The profile of the deformed droplet at steady state agrees well with the observation of Vu *et al.* [26].

In order to ensure that our results are independent of grid resolution, a grid convergence test is performed for a compound drop subjected to shear flow, in the absence of an electric field. The operating parameters are $\text{Re} = \text{Ca} = 0.2$, $\lambda = 1.0$, and $A = 0.5$. The temporal variation of the outer interface D for different grid refinement levels is presented in Fig. 2(c). The dimensionless sizes of the grid cell corresponding to the four chosen grids are 0.093, 0.046, 0.023, and 0.011, respectively. It is observed that the results converge with increasing refinement and the steady state deformation differs by only $\approx 0.1\%$ between levels 8 and 9. Therefore, the grid with refinement level 8 is selected for the present paper, to save computational time and cost without compromising the accuracy of the results.

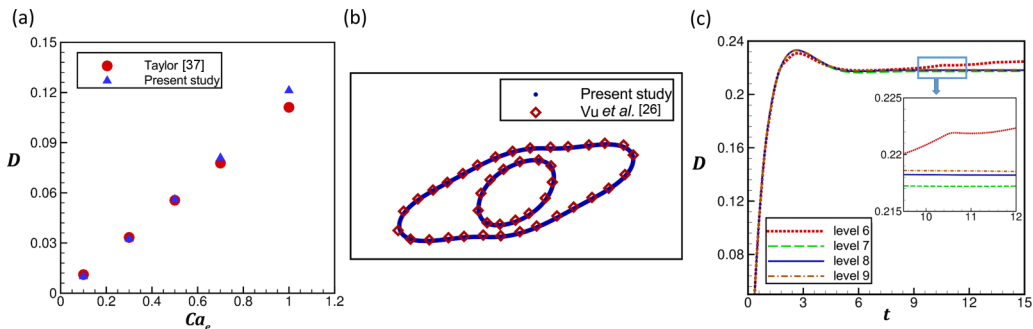


FIG. 2. (a) Deformation of a stationary droplet under a uniform electric field obtained from the present computations, along with the analytical predictions of Taylor [37]. (b) Steady shape of a compound droplet in shear flow, in the absence of an electric field, along with the numerical results of Vu *et al.* [26]. (c) Grid convergence test showing the deformation of the outer interface of a compound droplet for different refinement levels.

III. RESULTS AND DISCUSSION

We begin our paper on the dynamics of a compound droplet in liquid-liquid systems by briefly examining the effect of shear on the droplet morphology, in the absence of electric field. Subsequently, we explore the influence of the applied electric field with the assumption of perfect dielectric as well as leaky dielectric fluids. A large set of parameters falls under consideration, and in the results that follow we have fixed the values of Ca , Re , η , λ , and A at 0.2, 0.2, 1.0, 1.0, and 0.5 throughout the entire paper, unless mentioned otherwise. A typical example of such a system corresponds to a silicone oil droplet suspended in castor oil or vice versa. The effects of these hydrodynamic parameters on the dynamics of compound droplets in shear flow have been investigated by a host of researchers [25,26]. In the present paper, we focus on the electro-hydrodynamics of the adopted system and study extensively the impact of the electrical properties as well as the applied electric field on the flow behavior and its associated dynamics.

A. Without electric field

We initiate our investigation by examining the dynamics of a compound drop in shear flow in the absence of an electric field. Figures 3(a) and 3(b) present the influence of Ca on the steady state deformation D and orientation θ of both the inner and outer droplet interface, respectively. Additionally, the variation of minimum separation distance d_{\min} with Ca is shown in Fig. 3(c).

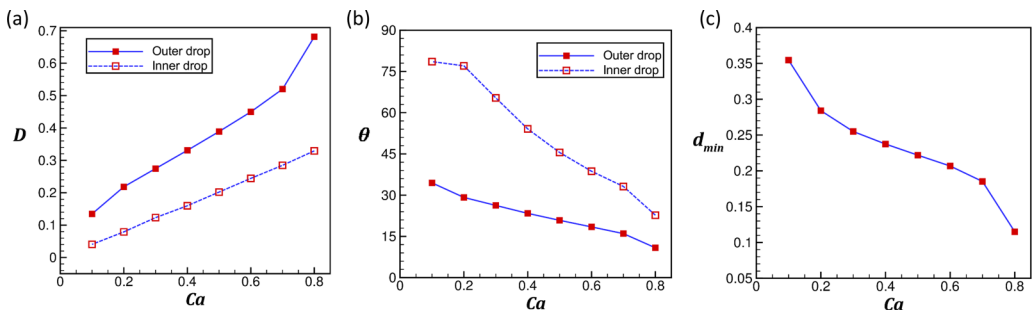


FIG. 3. Effect of capillary number Ca on the (a) deformation parameter D , (b) orientation angle θ , and (c) minimum separation distance d_{\min} .

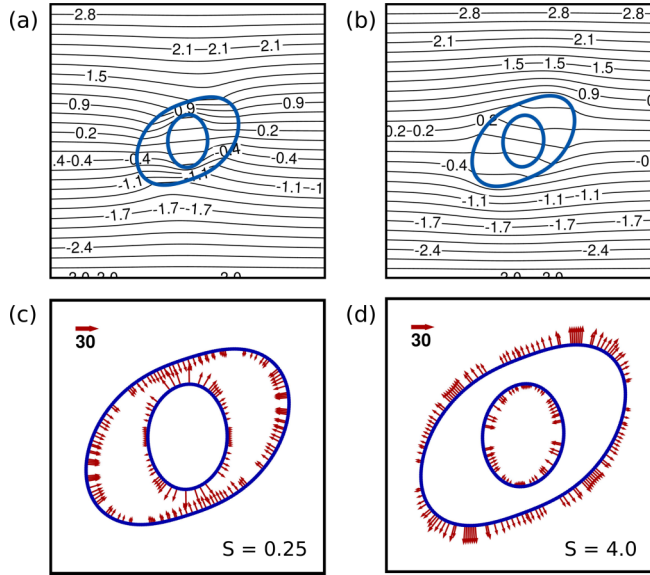


FIG. 4. (a), (b) Isocontour lines of the electric potential for $S = 0.25$ and 4.0 , respectively. (c), (d) The electric force acting at the interfaces of the compound droplet for $S = 0.25$ and 4.0 , respectively. Only selected force vectors are plotted to maintain clarity. The reference vector represents a force magnitude of 30 in nondimensionalized units. The Ca_e is fixed at 1.0 .

It can be observed from Fig. 3(a) that the deformation of both the inner and outer interfaces increases with increase in Ca . The deformation of the inner droplet is significantly smaller than the outer droplet. This can be attributed to the fact that the smaller curvature of the inner drop enhances the influence of interfacial force. In other words, the effective capillary number for the inner drop $Ca_{\text{inner}} = \left(\frac{r_i}{r_o}\right) \frac{\mu_e Gr_o}{\Gamma} = A Ca$, where $A = 0.5$. Furthermore, both the inner and outer droplets align themselves in the direction of imposed flow as Ca is increased, as illustrated in Fig. 3(b). As a consequence, the inner and outer interfaces approach each other and the minimum distance separating them decreases. These results corroborate with the predictions from previous studies in literature [25,26].

B. Perfect dielectric system

We now explore the influence of the electric field on compound droplets by considering the fluids to be perfect dielectric. The applied electric field produces stresses, known as Maxwell stresses, which act in addition to the influence of viscosity and surface tension. The magnitude of the polarization forces, arising out of the Maxwell stresses, is proportional to the contrast of permittivity between the two phases and squared magnitude of the applied electric field strength ($\mathbf{f}_e = -\frac{1}{2} \mathbf{E} \cdot \nabla \epsilon$). The electric force is directed from the medium of higher permittivity to lower permittivity and acts only at the interface, as the permittivity gradient exists only across the interface. Additionally, the polarization force is always locally perpendicular to the interface.

Figure 4 compares the polarization forces acting across the fluid interfaces for $S = 0.25$ and 4.0 , fixing $Ca_e = 1.0$. The electric forces prevailing in the two systems ($S = 0.25$ and 4.0) are inhomogeneous in nature, owing to local variation of the electric field strength. In the absence of any drop phase, a spatially uniform electric field is generated with lines of constant potential parallel to the channel walls. Due to the presence of the compound drop, the uniform electric field is interrupted, as shown in Figs. 4(a) and 4(b). The disparity in the dielectric permittivity between the continuous fluid (as well as inner fluid) and outer fluid causes the isopotential lines to be nonuniformly spaced. The higher spacing between the isopotential lines signifies regions of

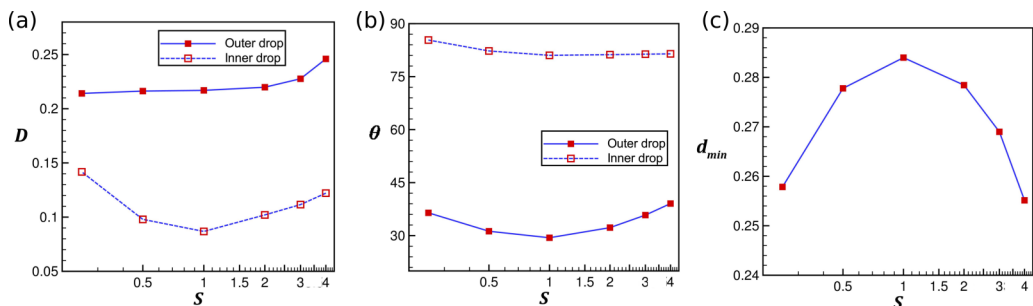


FIG. 5. Effect of permittivity ratio S on the (a) deformation parameter D , (b) orientation angle θ , and (c) minimum separation distance d_{min} . The electric capillary number Ca_e is fixed at 1.0.

lower electric field intensity. For the compound drop with $S = 0.25$, the outer fluid region possesses high electric field intensity. However, low electric field intensity can be identified in the inner fluid region and on the top and bottom of the outer droplet [as observed in Fig. 4(a)]. In contrast, for the case of $S = 4.0$ [depicted in Fig. 4(b)], low electric field intensity prevails in the outer fluid region, with diverged isopotential lines. The continuous fluid region contains significantly higher electric field intensity. However, the direction of the electric forces is different between the conditions of $S > 1.0$ and $S < 1.0$, as shown in Figs. 4(c) and 4(d). For $S < 1.0$, the electric forces acting at the interface of the outer droplet are compressive in nature, while electric forces acting at the interface of the inner droplet are tensile in nature, as observed in Fig. 4(c) for $S = 0.25$. In contrast, for $S > 1.0$, the electric forces acting at the interface of the outer droplet are tensile in nature, while electric forces acting at the interface of the inner droplet are compressive in nature, as observed in Fig. 4(d) for $S = 4.0$.

A parametric study of the variation of S on the drop morphology is carried out in Fig. 5. The Ca_e is kept fixed at 1.0 and the effect of S on the deformation parameter D , orientation angle θ , and minimum separation distance d_{min} is examined. The dotted lines represent the parameters for the inner drop and the solid lines denote the outer drop in both Figs. 5(a) and 5(b). It is observed from Fig. 5(a) that for the outer drop the deformation is largely insensitive to variation of S , when $S < 1.0$. As S is increased beyond unity, the outer droplet deformation is enhanced. However, the inner drop deformation is amplified when S is either increased or decreased beyond unity. Figure 5(b) depicts that the outer droplet tends to orient itself at a lower angle to the imposed shear flow. In contrast, the orientation of the inner droplet remains largely insensitive to the variation of S with a preferred alignment towards the electrodes. The separation between the interfaces decreases, when S is either increased or decreased beyond unity, as shown in Fig. 5(c).

In order to explain the aforementioned observations, we note here that the magnitude of the electric forces acting at the interface depends both on the relative permittivity contrast as well as the local electric field intensity. For the outer droplet, the polarization forces are strong around the equatorial region of the interface. The overall electric force magnitude ($|E|$) is significantly lower for $S < 1.0$. As a consequence, the deformation of the outer droplet is less sensitive to variation of S , when $S < 1.0$. On the other hand, the outer droplet deformation increases, when S is progressively increased beyond unity. For the inner droplet, the polarization forces are stronger at the poles, when $S < 1.0$. This leads to a higher deformation of the inner droplet under such condition. Furthermore, due to the strong pulling action at the poles, the inner droplet is oriented towards the electrodes, characterized by the high magnitude of θ . The outer drop, owing to its larger size, experiences a higher impact of the incident flow, thereby leading to significantly lower incident angles. However, as the permittivity contrast is increased, a preferred orientation towards the electrodes is observed, due to the augmented electric forces at the interface. Additionally, as S is progressively increased or decreased beyond unity, the enhanced deformation of the inner or outer interfaces (or both) reduces the minimum interfacial distance d_{min} .

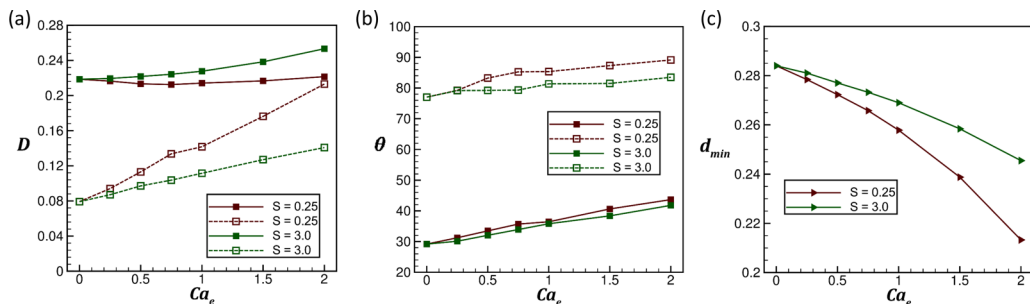


FIG. 6. Effect of electric capillary number Ca_e on the (a) deformation parameter D , (b) orientation angle θ , and (c) minimum separation distance d_{min} for $S = 0.25$ and 3.0 . The dotted lines represent the parameters for the inner drop and the solid lines denote the outer drop in both (a) and (b).

Figure 6 illustrates the effect of electric capillary number (Ca_e) on the droplet morphology and orientation. It is observed that both the inner and outer droplet deformations increase with increase in Ca_e , which can be attributed to the increasing strength of the electric forces at the interface. Additionally, both the inner and outer droplets tend to orient in the direction of electric field, due to the stronger effect of the applied field. Figure 6(c) shows that the minimum distance between the two interfaces of the compound droplet decreases with increase in Ca_e , owing to the enhanced deformation of both the inner and outer interfaces.

C. Leaky dielectric system

In this section, we investigate the influence of electric field on the dynamics of compound droplets by considering the fluids to be leaky dielectric. Due to the small but finite electrical conductivity of the liquids, the leaky dielectric model allows the presence of both normal and tangential electric stresses at the droplet interface. Hence, we expect significant differences in the dynamics of the droplets between perfect dielectric and leaky dielectric systems. The electric Reynolds number, defined in Eq. (11) as $Re_e = \frac{\epsilon_c G}{\sigma_c} = \left(\frac{\epsilon_c / \sigma_c}{(r_o / G r_o)} \right) = \frac{t_e}{t_f}$, is the ratio of the time scale of charge relaxation (electric time scale t_e) to the flow time scale t_f . Under the condition of $t_e < t_f$, volumetric charge does not exist in the bulk fluid and the charges accumulate at the interface, instantly satisfying the assumption of leaky dielectric fluids. In our present paper, we have fixed the value of $Re_e = 0.1$ for the entire investigation using leaky dielectric fluids. The chosen value of Re_e is similar to the typical values used in literature [6,8,18]. Additionally, we have explored with different values of Re_e and observed that the dynamics remain insensitive to the value of Re_e for $Re_e < 1.0$.

We consider two distinct (R, S) pairs of leaky dielectric fluids with values of $(2.0, 0.5)$ and $(0.5, 2.0)$, denoted as systems A and B, respectively. System A represents a compound droplet the outer droplet of which has a higher conductivity, but lower permittivity than the continuous (and inner drop) fluid. On the other hand, system B represents a compound drop having a lower conductivity and higher permittivity of the outer droplet, in comparison to the continuous (and inner drop) fluid. Both these systems are chosen as representative examples rather than values provided by a specific fluid-fluid configuration. In the sole presence of an electric field, a two-dimensional droplet may deform either along the direction of the electric field or perpendicular to it, depending on the magnitude of a discriminating function, given by $f = R^2 + R + 1 - 3S$ [38]. Corresponding to the (R, S) values for system A, a positive magnitude of f is obtained, indicating prolate deformation. On the other hand, a negative value of f is obtained for system B, thereby signaling oblate deformation. Hence, the choice of these reflective (R, S) values allows us to contrast the dynamical response of compound droplets for these fundamentally different systems and elucidate the underlying causes for the differing behavior.

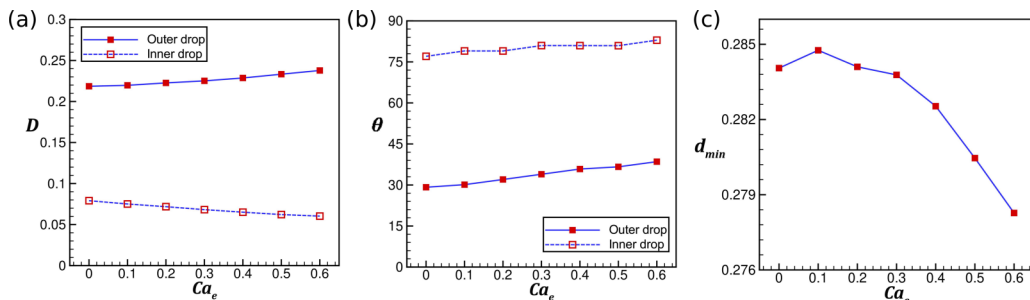


FIG. 7. Effect of electric capillary number Ca_e on the (a) deformation parameter D , (b) orientation angle θ , and (c) minimum separation distance d_{\min} for system A.

Figure 7 presents the variation of D , θ , and d_{\min} with Ca_e for system A. It can be clearly perceived that the deformation of the inner and outer droplets shows a contrasting behavior with change in Ca_e . For the outer droplet, the deformation shows a monotonous increase with increase in Ca_e . In contrast, the inner droplet undergoes a reduction in deformation as Ca_e is enhanced. However, the magnitude of θ shows a continuous increase for both the inner and outer droplets at progressively higher Ca_e . This signifies that the droplets orient against the flow direction as the influence of electric field is enhanced for both the systems under consideration. Furthermore, d_{\min} decreases due to the enhanced deformation of the outer droplet.

The influence of Ca_e on the morphology of compound droplets for system B is shown in Fig. 8. It is observed that the deformation shows an increasing trend for both the inner and outer droplets. Furthermore, both the inner and outer droplets tend to orient themselves with the flow, as depicted by the decrease in θ at higher Ca_e . Similar to the case of system A, d_{\min} decreases with increase in Ca_e . It is to be noted here that the magnitude of deformation for compound drops of system B is significantly higher than system A. As a consequence, the separation distance d_{\min} is notably lower in system B, in comparison to system A.

The differing behavior of the drops for the systems under consideration can be understood by closely examining the charges accumulated and the electric forces at the interfaces. The net electric forces for leaky dielectric fluids can be categorized into the Coulombic component ($q\mathbf{E}$) exerted on the free charges and the polarization component acting on the bound charges ($-\frac{1}{2}\mathbf{E} \cdot \mathbf{E}\nabla\epsilon$). As mentioned in Sec. III B, the polarization forces are directed from the medium of higher permittivity to lower permittivity and act only at the interface. On the other hand, the Coulombic forces point in the direction of the applied field, when the accumulated charge is positive in nature. In contrast, the Coulombic forces act opposite to the applied electric field, when the accumulated charge is negative. Furthermore, the assumption of leaky dielectric fluids guarantees that the charges are concentrated

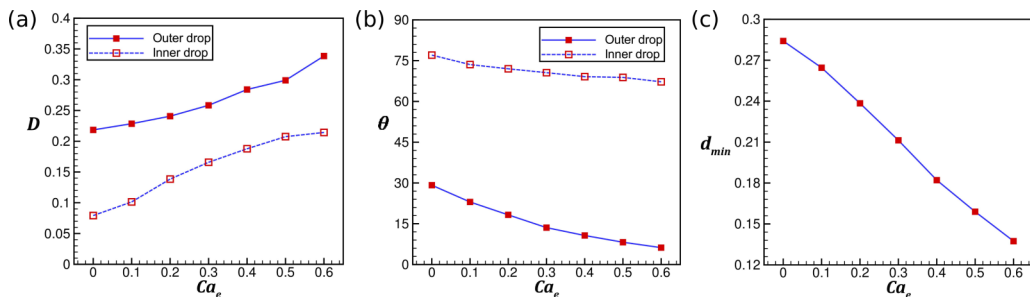


FIG. 8. Effect of electric capillary number Ca_e on the (a) deformation parameter D , (b) orientation angle θ , and (c) minimum separation distance d_{\min} for system B.

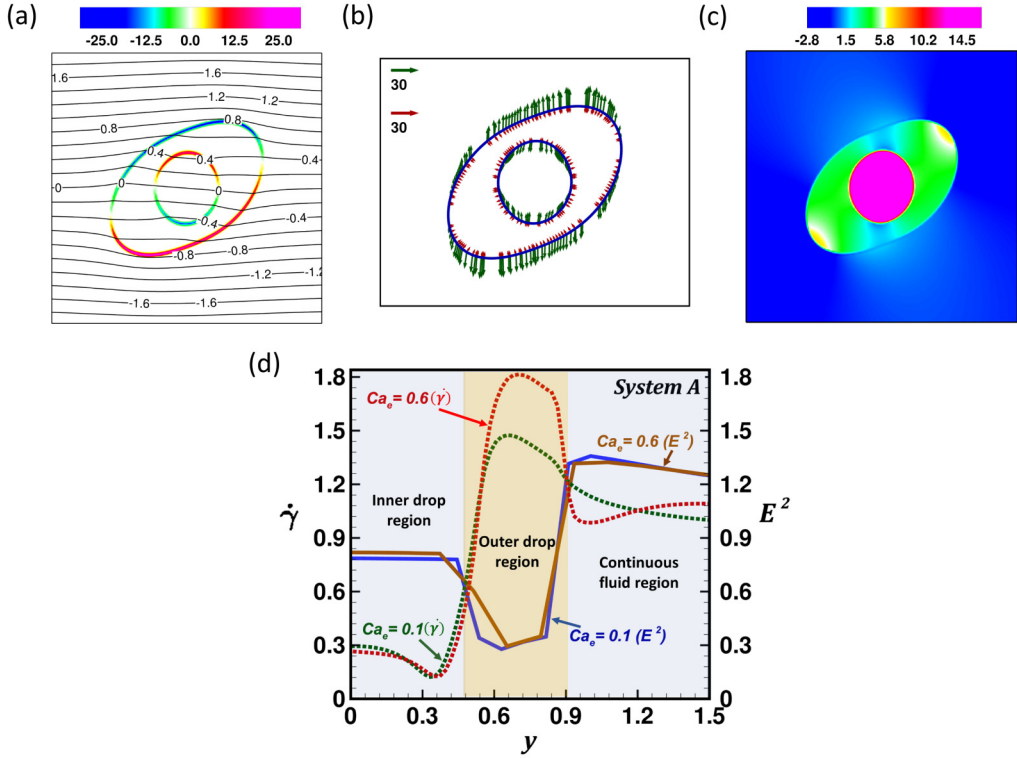


FIG. 9. (a) The distribution of charge accumulated at the interface along with isocontours of electric potential for system A. (b) The electric forces acting at the interface for system A. The Coulombic forces acting on the free charges ($q\mathbf{E}$) are shown in green color, while the polarization forces ($-\frac{1}{2}\mathbf{E} \cdot \nabla\epsilon$) are depicted in red color. Only selected force vectors are plotted to maintain clarity. (c) The pressure distribution in the compound drop for system A. The value of Ca_e is fixed at 0.6. (d) The distribution of shear rate along the vertical direction (y axis) for system A, computed at the pole of the inner droplet, for $Ca_e = 0.1$ and 0.6.

only at the interface, while the bulk remains free of charges. As a result, the Coulombic forces also act only at the drop interface.

Figures 9(a) and 9(b) illustrate the charge accumulation, the distribution of electric forces, and the pressure field in a compound droplet for system A. The upper portion of the outer drop becomes negatively charged, whereas the lower portion is positively charged. In contrast, the charge accumulation on the inner drop is opposite in nature. It is to be noted that the magnitude of the Coulombic force outweighs the polarization force for both the inner and outer interfaces. The Coulombic force varies spatially along the interface due to the local variation of the charge density and electric field strength. Figure 9(d) presents the local variation of squared field strength E^2 and shear rate $\dot{\gamma}$ with Ca_e , computed along a vertical axis drawn near the pole of the inner drop. It can be observed that the magnitude of $\dot{\gamma}$ decreases inside the inner drop, when Ca_e is increased from 0.1 to 0.6. In contrast, E^2 increases as Ca_e is enhanced, within the region of the inner drop. The cumulative effect of the hydrodynamic and electric forces leads to reduction in the inner droplet deformation with increase in Ca_e . Contrastingly, $\dot{\gamma}$ increases by a significant amount in the outer drop, as Ca_e is enhanced, thereby leading to higher deformation of the outer drop. It can be clearly perceived that the pressure in the outer drop attains a minimum near the “throat” section, wherein the interface separation is minimum. With increase in Ca_e , the magnitude of d_{\min} decreases, owing to the combined effect of deformation and orientation of both the inner and outer droplets. Furthermore,

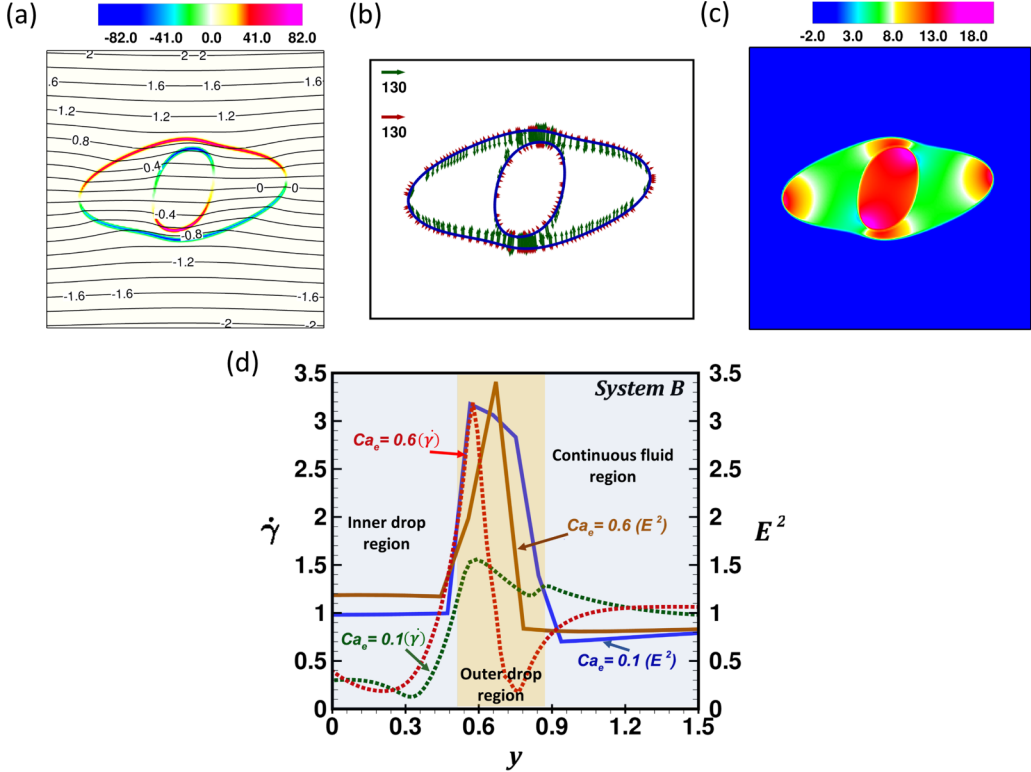


FIG. 10. (a) The distribution of charge accumulated at the interface along with isocontours of electric potential for system B. (b) The electric forces acting at the interface for system B. The Coulombic forces acting on the free charges ($q\mathbf{E}$) are shown in green color, while the polarization forces ($-\frac{1}{2}\mathbf{E} \cdot \nabla \epsilon$) are depicted in red color. Only selected force vectors are plotted to maintain clarity. (c) The pressure distribution in the compound drop for system B. The value of Ca_e is fixed at 0.6. (d) The distribution of shear rate along the vertical direction (y axis) for system B, computed at the pole of the inner droplet, for $Ca_e = 0.1$ and 0.6.

the throat region is extended, when the magnitude of Ca_e is increased. As a result, the inner droplet preferably orients at a higher angle with increasing Ca_e .

Figures 10(a), 10(b) and 10(c) present the charge accumulation, the distribution of electric forces, and the pressure field in a compound droplet for system B. The upper half of the outer drop is positively charged, whereas the lower part is negatively charged. As a consequence, the outer drop experiences a repulsion from the electrodes and deforms in the axial direction. The strength of the Coulombic forces increase with increase in Ca_e , thereby further aligning the outer drop in the direction of the incident shear flow. The charge distribution in the inner drop is opposite to the outer drop. Figure 10(d) presents the local variation of E^2 and $\dot{\gamma}$ with Ca_e , computed along a vertical axis drawn near the pole of the inner drop. It can be observed that both $\dot{\gamma}$ and E^2 increase with increase in Ca_e . As a consequence, the deformation of the inner droplet is augmented, as Ca_e is increased. The Coulombic forces acting on the inner droplet are tensile in nature and the intensity is higher at the poles. The tensile pull exerted by the electric field tends to elongate the inner droplet towards the electrodes. However, this elongation is resisted by the region of high pressure created in the thin “neck” region separating the inner and outer interfaces. As d_{\min} decreases with increase in Ca_e , the high pressure region prevailing near the thin neck region is enhanced. Hence, the inner drop orients towards the incident flow with increasing Ca_e , thereby lowering θ . It is to be noted here that the magnitude of Coulombic forces generated for system B is much higher than system A. As a result, the corresponding deformations of both the inner and outer interfaces are significantly higher for

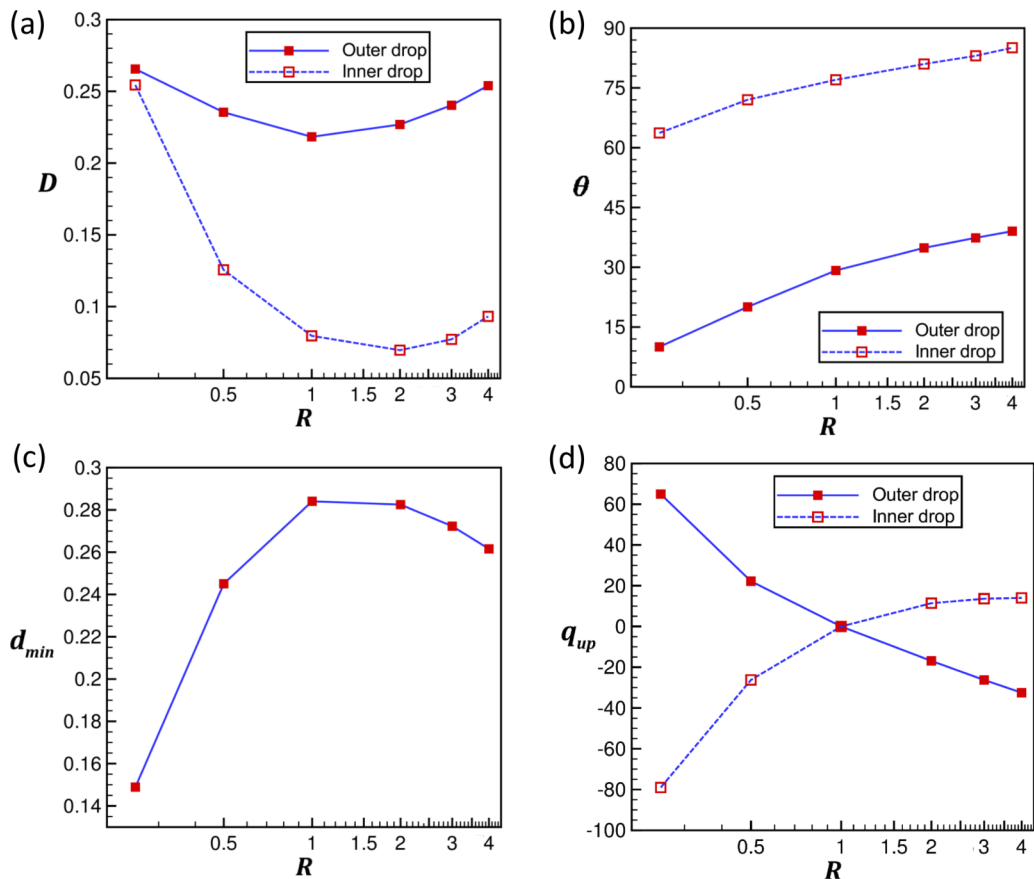


FIG. 11. Effect of conductivity ratio R on the (a) deformation parameter D , (b) orientation angle θ , (c) minimum separation distance d_{min} , and (d) maximum charge accumulated at the upper half of the drop interfaces q_{up} . The Ca_e is fixed at 0.5.

system B, in comparison to system A. Accordingly, the values of d_{min} are notably lower for system B than system A.

We further investigate the influence of the conductivity ratio R , keeping the Ca_e and S fixed at 0.5 and 1.0, respectively. Under such condition, the polarization forces vanish due to the absence of permittivity contrast between the fluids. The variation of D , θ , and d_{min} with increasing R is depicted in Fig. 11. It can be clearly perceived that with increase in R , the deformation D decreases for $R < 1.0$ and increases for $R > 1.0$, for both the inner and outer droplets. The angle of orientation θ increases monotonously for both inner and outer droplets with increase in R . The magnitude of d_{min} decreases, when R is either increased or decreased beyond unity. The modification of the droplet behavior at varying R can be ascribed to the fact that the nature of charge accumulation is fundamentally altered due to the change in R , as illustrated in Fig. 11(d). The contrasting nature of charge accumulation for both the inner and outer interfaces and its variation with changing R effectively modifies the behavior of the Coulombic forces, thereby remarkably altering the dynamics of the compound droplets.

D. Breakup of compound droplets

The steady state deformation of compound droplets under the combined influence of electric field and shear flow depends on a delicate balance between hydrodynamic and electric stresses. However,

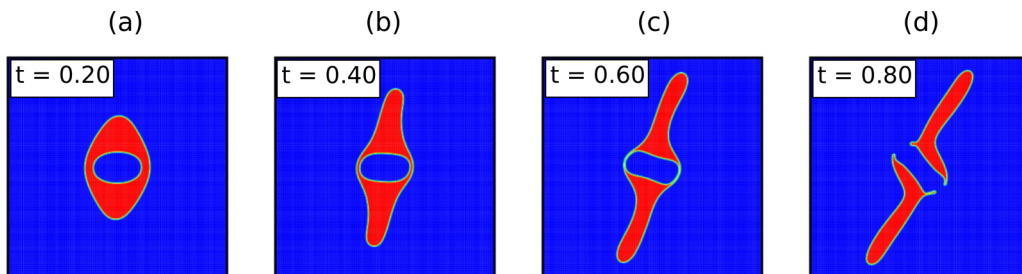


FIG. 12. Temporal snapshots showing the breakup of a compound droplet for system A. The image sequences are presented for (a) $t = 0.20$, (b) $t = 0.40$, (c) $t = 0.60$, and (d) $t = 0.80$. The value of Ca_e is taken as 12.0.

under certain circumstances, this fine balance may fail, leading to breakup of the compound droplets. In the present section, we briefly demonstrate the breakup of compound droplets by suitably tuning the electric field strength. For the case of drops of system A, as shown in Fig. 12, the inner drop elongates along the flow direction, whereas the outer drop deforms towards the electrodes, albeit in a slightly inclined manner. A swiftly thinning region can be clearly noticed around the equatorial ends of the drop, wherein both the interfaces close in onto each other. Eventually, the gap between the two interfaces becomes negligible ($d_{\min} \rightarrow 0$) and the thin shell ruptures to release the inner fluid.

In contrast, the deformation of the inner and outer droplets of system B is completely opposite in nature to that of system A, as depicted in Fig. 13. Although a similar thinning shell can be observed, the location of decreasing d_{\min} is found to be near the uppermost and lowermost tips of the deformed droplet. Subsequently, the interfaces touch each other, leading to droplet breakup. Herein, we highlight the fact that the breakup of droplets of system B occurs at a significantly lower Ca_e than system A. This can be readily explained by referring to the fact that the magnitude of electric forces generated is much higher for drops of system B than system A.

The differing breakup phenomenon of the droplets reveals that for applications requiring stability of the compound droplets in EHD flow setup, the configuration pertaining to system A is preferable. On the other hand, when the facile breakup of the droplet is desired, the setup corresponding to system B is more beneficial. Here, in the present paper, we note that the final disintegration of the thin liquid shell leading to breakup is essentially numerical. This is due to the fact that the physics that governs the shell breakup involves molecular processes and requires multiscale modeling, which hopefully will be possible in the future.

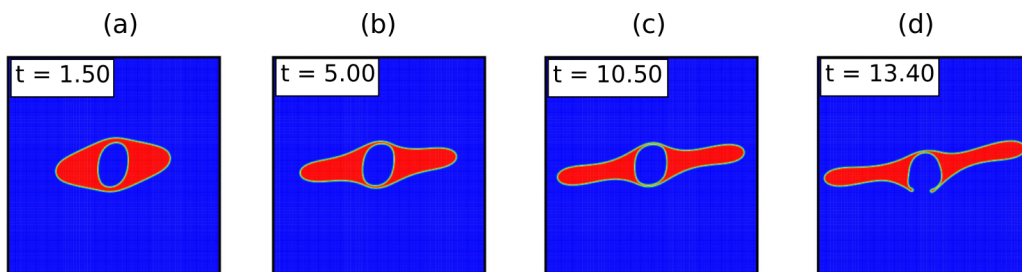


FIG. 13. Temporal snapshots showing the breakup of a compound droplet for system B. The image sequences are presented for (a) $t = 1.50$, (b) $t = 5.00$, (c) $t = 10.50$, and (d) $t = 13.40$. The value of Ca_e is taken as 0.9.

The error introduced due to numerical clipping of the interface tends to be of the order of the smallest grid cell used in the simulations. Additionally, to accurately capture the rupture of the compound droplet and the postbreakup dynamics, the use of full three-dimensional simulations is preferred, which falls beyond the scope of the present paper.

E. Caveats and utility of the paper

An important assumption in the present paper is that the simulations are performed in a two-dimensional framework. Owing to this simplification, obtaining an exact match between the computations and experimental results is a difficult task. However, the 2D numerical analysis can predict the phenomenon studied in a realistic microfluidic setup (Couette flow system) with reasonable accuracy, when the third dimension (which is perpendicular to the plane of flow) is considered to be large enough. Accordingly, the 2D numerical model has been employed extensively in prior literature for capturing the essential physics related to the dynamics of droplets in shear flows [8,39,40]. The 2D and 3D electro-hydrodynamics of droplets also possess several similarities. In the sole presence of a uniform electric field, the EHD induced flows in a plane parallel to the direction of the field are identical for 2D and 3D droplets [40]. Therefore, it is reasonable to expect that the current two-dimensional framework will provide realistic insight into the dynamics of droplets in shear flow and maintain a notable degree of physical significance. The extension of the current paper, by adopting a full 3D configuration, can be taken up in a future study. The dynamic mesh refinement technique [41] may be employed for performing the simulations, in order to optimize the computational performance and maintain reasonable grid resolution.

It is to be noted here that the EHD incorporated Couette flow system considered in our paper provides an ideal platform to study the interplay of imposed shear and electric field on droplet morphology and breakup. This simplistic configuration allows us to focus on the rich dynamics of droplets subjected to the combined influence of shear and electric forces, while avoiding additional complexities arising out of droplet translation and migration. The present paper provides valuable insight for understanding the dynamical response of compound droplets and elucidates conditions for controlled deformation and breakup. In real world applications, compound droplets may act as an encapsulated carrier for targeted delivery and screening purposes. The present paper highlights the importance of EHD based technologies for tunable control over compound droplets [42].

IV. CONCLUSIONS

The present paper investigates the dynamics of compound droplets under the combined influence of an external electric field and imposed shear flow. The paper focuses on the deformation and morphology of the compound droplet and briefly explores the droplet breakup. The coupled electro-hydrodynamic equations are solved in a two-dimensional finite volume framework, considering the fluids as either perfect dielectric or leaky dielectric. The interface is captured using the volume-of-fluid method. The results obtained from the present paper are summarized in this section.

The paper reveals that in the case of dielectric fluids, the deformation of both the inner and outer droplets is enhanced as the electric capillary number Ca_e is increased. The variation of permittivity ratio S can lead to either reduction or augmentation of the inner drop deformation. The polarization force engendered by the applied electric field acts normal to the interface, and the direction of the force is dictated by the magnitude of S . The variance in electric permittivity across the inner and outer droplet interfaces leads to a spatial variation of the the field intensity. As a consequence, the steady state orientation of the droplet can be modulated by variation of the permittivity contrast between the fluids.

Systems of leaky dielectric fluids have also been explored, and in particular two systems have been analyzed in detail. Depending on the relative magnitude of conductivity ratio R and permittivity ratio S , the two configurations have been denoted as system A and system B. It is observed that the

deformation of both the inner and outer droplet can be manipulated by variation of Ca_e . The droplets of system A tend to orient against the flow direction, whereas in the case of system B, alignment along the flow direction is preferred. Interestingly, the charge accumulation at the interfaces for both the systems presents a contradictory picture, which fundamentally alters the direction of the Coulombic forces for the two systems under consideration. The conductivity ratio R controls the magnitude of charge accumulated at the interfaces.

Finally, the breakup of compound droplets is demonstrated for droplets of both system A and B. It is observed that droplets corresponding to system A are more stable than system B in the presence of the electric field. In contrast, droplets of system B can be ruptured at relatively lower magnitude of the applied electric field. The differing nature of breakup can be attributed to the striking disparity in the magnitude as well as nature of Coulombic forces between the two systems considered in our paper.

The observations from the present analysis may be beneficial for electric field mediated applications to provide tunable control over the behavior of compound droplets. This paper may be further extended to investigate the influence of time varying or alternating electric fields.

The data that support the findings of this paper are available from the corresponding author upon reasonable request.

ACKNOWLEDGMENT

G.B. acknowledges indebtedness to the J. C. Bose National Fellowship of SERB, Government of India.

-
- [1] A. Utada, E. Lorenceau, D. Link, P. Kaplan, H. Stone, and D. Weitz, Monodisperse double emulsions generated from a microcapillary device, *Science* **308**, 537 (2005).
 - [2] D. Lee and D. A. Weitz, Double emulsion-templated nanoparticle colloidosomes with selective permeability, *Adv. Mater.* **20**, 3498 (2008).
 - [3] S.-H. Kim, H. C. Shum, J. W. Kim, J.-C. Cho, and D. A. Weitz, Multiple polymersomes for programmed release of multiple components, *J. Am. Chem. Soc.* **133**, 15165 (2011).
 - [4] A. R. Abate, C.-H. Chen, J. J. Agresti, and D. A. Weitz, Beating Poisson encapsulation statistics using close-packed ordering, *Lab Chip* **9**, 2628 (2009).
 - [5] A. Abate and D. Weitz, High-order multiple emulsions formed in poly (dimethylsiloxane) microfluidics, *Small* **5**, 2030 (2009).
 - [6] M. P. Borthakur, G. Biswas, and D. Bandyopadhyay, Dynamics of drop formation from submerged orifices under the influence of electric field, *Phys. Fluids* **30**, 122104 (2018).
 - [7] B. Nath, G. Biswas, A. Dalal, and K. C. Sahu, Cross-stream migration of drops suspended in poiseuille flow in the presence of an electric field, *Phys. Rev. E* **97**, 063106 (2018).
 - [8] B. Nath, G. Biswas, and A. Dalal, Influence of electric field on deformation of a drop in shear flow, *Phys. Fluids* **31**, 042102 (2019).
 - [9] O. A. Basaran, Small-scale free surface flows with breakup: Drop formation and emerging applications, *AIChE J.* **48**, 1842 (2002).
 - [10] Y. Wu and R. L. Clark, Electrohydrodynamic atomization: a versatile process for preparing materials for biomedical applications, *J. Biomater. Sci., Polym. Ed.* **19**, 573 (2008).
 - [11] S. Sadhal and H. Oguz, Stokes flow past compound multiphase drops: The case of completely engulfed drops/bubbles, *J. Fluid Mech.* **160**, 511 (1985).
 - [12] E. Rushton and G. Davies, Settling of encapsulated droplets at low Reynolds numbers, *Int. J. Multiphase Flow* **9**, 337 (1983).
 - [13] S. Kawano, A. Shirai, and S. Nagasaka, Deformations of thin liquid spherical shells in liquid-liquid-gas systems, *Phys. Fluids* **19**, 012105 (2007).

- [14] R. E. Johnson and S. Sadhal, Fluid mechanics of compound multiphase drops and bubbles, *Annu. Rev. Fluid Mech.* **17**, 289 (1985).
- [15] H. Stone and L. Leal, Breakup of concentric double emulsion droplets in linear flows, *J. Fluid Mech.* **211**, 123 (1990).
- [16] P. Stroeve and P. P. Varanasi, An experimental study on double emulsion drop breakup in uniform shear flow, *J. Colloid Interface Sci.* **99**, 360 (1984).
- [17] K. A. Smith, J. M. Ottino, and M. O. Olvera de la Cruz, Encapsulated Drop Breakup in Shear Flow, *Phys. Rev. Lett.* **93**, 204501 (2004).
- [18] S. Mandal, A. Bandopadhyay, and S. Chakraborty, The effect of uniform electric field on the cross-stream migration of a drop in plane poiseuille flow, *J. Fluid Mech.* **809**, 726 (2016).
- [19] S. Sadhal *et al.*, Growth and collapse of translating compound multiphase drops: Analysis of fluid mechanics and heat transfer, *J. Fluid Mech.* **179**, 105 (1987).
- [20] P. Gao and J. J. Feng, Spreading and breakup of a compound drop on a partially wetting substrate, *J. Fluid Mech.* **682**, 415 (2011).
- [21] M. P. Borthakur, G. Biswas, and D. Bandyopadhyay, Dynamics of deformation and pinch-off of a migrating compound droplet in a tube, *Phys. Rev. E* **97**, 043112 (2018).
- [22] Y. Chen, X. Liu, and M. Shi, Hydrodynamics of double emulsion droplet in shear flow, *Appl. Phys. Lett.* **102**, 051609 (2013).
- [23] Y. Chen, X. Liu, and Y. Zhao, Deformation dynamics of double emulsion droplet under shear, *Appl. Phys. Lett.* **106**, 141601 (2015).
- [24] L. Zhu and F. Gallaire, Bifurcation Dynamics of a Particle-Encapsulating Droplet in Shear Flow, *Phys. Rev. Lett.* **119**, 064502 (2017).
- [25] H. Hua, J. Shin, and J. Kim, Dynamics of a compound droplet in shear flow, *Int. J. Heat Fluid Flow* **50**, 63 (2014).
- [26] T. V. Vu, L. V. Vu, B. D. Pham, and Q. H. Luu, Numerical investigation of dynamic behavior of a compound drop in shear flow, *J. Mech. Sci. Technol.* **32**, 2111 (2018).
- [27] J.-W. Ha and S.-M. Yang, Fluid dynamics of a double emulsion droplet in an electric field, *Phys. Fluids* **11**, 1029 (1999).
- [28] A. Behjatian and A. Esmaeeli, Electrohydrodynamics of a compound drop, *Phys. Rev. E* **88**, 033012 (2013).
- [29] A. Behjatian and A. Esmaeeli, Transient electrohydrodynamics of compound drops, *Acta Mech.* **226**, 2581 (2015).
- [30] P. Soni, V. A. Juvekar, and V. M. Naik, Investigation on dynamics of double emulsion droplet in a uniform electric field, *J. Electrostat.* **71**, 471 (2013).
- [31] M. S. Abbasi, R. Song, J. Kim, and J. Lee, Electro-hydrodynamic behavior and interface instability of double emulsion droplets under high electric field, *J. Electrostat.* **85**, 11 (2017).
- [32] M. P. Borthakur, G. Biswas, and D. Bandyopadhyay, Formation of liquid drops at an orifice and dynamics of pinch-off in liquid jets, *Phys. Rev. E* **96**, 013115 (2017).
- [33] J. Brackbill, D. B. Kothe, and C. Zemach, A continuum method for modeling surface tension, *J. Comput. Phys.* **100**, 335 (1992).
- [34] S. Popinet, A quadtree-adaptive multigrid solver for the Serre-Green-Naghdi equations, *J. Comput. Phys.* **302**, 336 (2015).
- [35] S. Popinet, Gerris: A tree-based adaptive solver for the incompressible Euler equations in complex geometries, *J. Comput. Phys.* **190**, 572 (2003).
- [36] M. Balla, M. K. Tripathi, and K. C. Sahu, A numerical study of a hollow water droplet falling in air, *Theor. Comput. Fluid Dyn.* **34**, 133 (2020).
- [37] G. I. Taylor, Studies in electrohydrodynamics. I. The circulation produced in a drop by an electric field, *Proc. R. Soc. A* **291**, 159 (1966).
- [38] P. H. Rhodes, R. S. Snyder, and G. O. Roberts, Electrohydrodynamic distortion of sample streams in continuous flow electrophoresis, *J. Colloid Interface Sci.* **129**, 78 (1989).
- [39] B. Nath, M. P. Borthakur, and G. Biswas, Electric field induced dynamics of viscoplastic droplets in shear flow, *Phys. Fluids* **32**, 092110 (2020).

- [40] S. Santra, S. Mandal, and S. Chakraborty, Confinement effect on electrically induced dynamics of a droplet in shear flow, [Phys. Rev. E **100**, 033101 \(2019\)](#).
- [41] M. P. Borthakur, G. Biswas, D. Bandyopadhyay, and K. C. Sahu, Dynamics of an arched liquid jet under the influence of gravity, [Eur. J. Mech. B/Fluids **74**, 1 \(2019\)](#).
- [42] M. S. Abbasi, R. Song, S. Cho, and J. Lee, Electro-hydrodynamics of emulsion droplets: Physical insights to applications, [Micromachines **11**, 942 \(2020\)](#).